

New DNA-Interactive Manganese(II) Complex of Amidooxime: Crystal Structure, DFT Calculation, Biophysical and Molecular Docking Studies

Urmila Saha, Malay Dolai,* Gopinatha Suresh Kumar, Ray J. Butcher, and Saugata Konar

Cite This: <https://dx.doi.org/10.1021/acs.jced.0c00529>

Read Online

ACCESS |



Metrics & More

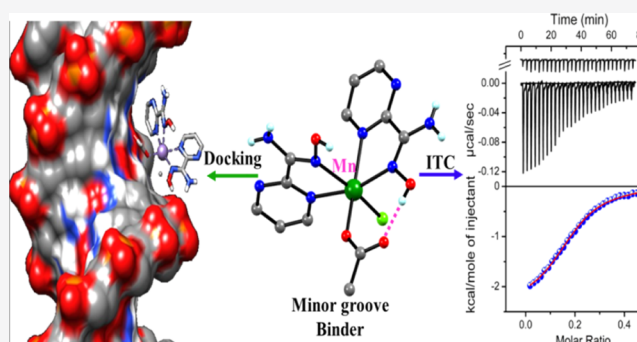


Article Recommendations



Supporting Information

ABSTRACT: A manganese(II) complex $[\text{Mn}^{\text{II}}(\text{HL}_1)_2(\text{Cl})(\text{CH}_3\text{COO})](1)$ based on the amidooxime ligand was synthesized and characterized by single-crystal X-ray diffraction studies, elemental analysis, UV-vis, and IR spectroscopy. The structural and spectral parameters were further supported using DFT/B3LYP. The complex (1) is mononuclear, having an octahedral geometry. The interaction of 1 with calf thymus DNA was investigated by spectroscopic and calorimetric techniques. The complex was found to interact with DNA through the groove-binding mode. From the isothermal titration calorimetry experiment, the binding constant between 1 and DNA was estimated to be $(4.39 \pm 0.01) \times 10^5 \text{ M}^{-1}$. The negative standard molar Gibbs energy change (ΔG^0) and positive entropy ($T\Delta S^0$) values obtained from the calorimetry study confirmed the spontaneity of 1-DNA complexation. Thermodynamic parameters also suggested that the process of interaction of 1 with DNA was entropy-driven. The molecular docking study revealed that 1 binds at G30, C29, T31, A14, and G13 base pairs of the DNA chain in the minor groove.



INTRODUCTION

Manganese is a crucial biologically relevant metal, especially for its active participation in the formation of various enzymes and proteins such as superoxide dismutase, glutamine synthetase, and so forth.^{1,2} Manganese is implicated for assisting the metabolism, neuro functions, balancing blood sugar, production of sex hormones, and calcium absorption. However, studies on the biological activity of manganese complexes are scarce.³ Manganese is found in the active site of a plethora of enzymes,^{4–6} anticancer agents (SC-52608), and MRI contrast reagents such as $[\text{Mn}(\text{dpdp})]^{4-}$ (dpdp = dipyridoxyldiphosphate) for detection of hepatocellular carcinomas.⁷ Furthermore, manganese complexes with diverse ligands are known to exhibit bactericidal^{8–10} and antiproliferative effects^{11,12} on several cancer cell lines and have antitumor activities.¹³ Consequently, the study of the bioactivity of novel manganese complexes has gained prime interest in the recent times. These observations have motivated the development of new manganese-based drugs.

In the recent past, investigation on the association of small molecules with nucleic acids has risen as functioning research at the interface of chemistry and molecular biology.¹⁴ DNA carries genetic information¹⁵ and is the prime cellular target of many drugs and small molecules, interfering with its function. DNA interacts with small molecules in three noncovalent ways: intercalation, groove binding, and external binding,^{16–22}

but a complex may also exhibit a mixed mode of binding. The structural changes induced in the DNA helix for these interactions may result in the disruption of the replication process and transcription events, eventually leading to apoptosis and cell death.²³ Therefore, a quantitative study of nucleic acid interaction with several proteins, enzymes, and drugs is essential for drug development.^{24,25} Fluorescence and chemiluminescence are widely used physicochemical tools for monitoring the interaction of different small molecules with DNA.²⁶ For the nonfluorescent nature of DNA, the direct use of the natural fluorescence emission properties of nucleic acids is not applicable.^{27,28} Therefore, an extrinsic fluorescent probe must be employed in the studies involving DNA.^{23,29}

On the other hand, studies on the bioactivity of the oxime-based manganese complexes are in their infant stage. Very few studies have been reported in recent years,^{16–18,30} and work on manganese complexes exhibiting bioactivity and DNA binding has attracted special attention recently.

Received: June 8, 2020

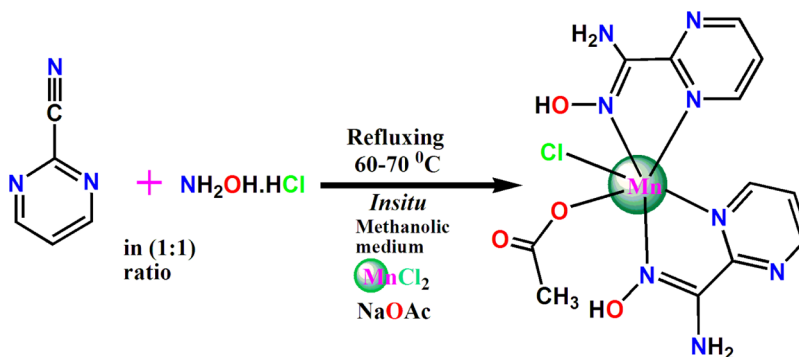
Accepted: September 28, 2020



Table 1. Sample Source, CAS Registry, and Initial Purity

material	chemical formula	CAS	supplier	purity (mass fraction)
2-pyrimidine carbonitrile	C ₅ H ₃ N ₃	14080-23-0	Merck, India	97%
manganese(II) chloride tetrahydrate	MnCl ₂ ·4H ₂ O	13446-34-9	Merck, India	≥98%
hydroxylaminehydrochloride	NH ₂ OH·HCl	5470-11-1	Merck, India	≥99.0%
sodium acetate	CH ₃ COONa	127-09-3	Merck, India	≥99.0%
deoxyribonucleic acid sodium salt from calf thymus	Calf thymus DNA	73049-39-5	Sigma-Aldrich	41.9 mol % G-C and 58.1 mol % A-T
bisbenzimidazole (Hoechst 33258)	C ₂₅ H ₂₄ N ₆ O·3HCl	23491-45-4	Sigma-Aldrich	≥98%
citric acidmonohydrate	HOC(COOH)(CH ₂ COOH) ₂ ·H ₂ O	5949-29-1	Sigma-Aldrich	≥99.0%
di-sodium hydrogen phosphate anhydrous	Na ₂ HPO ₄	7558-79-4	Merck, India	chemically pure
methanol	CH ₃ OH	67-56-1	Merck, India	≥99.8%
dimethyl Sulfoxide	(CH ₃) ₂ SO	67-68-5	Merck, India	≥99.9%
manganese complex (1)	C ₁₂ H ₁₅ ClMnN ₈ O ₄		Synthesis	99%

Scheme 1. Synthetic Scheme of Complex 1



Herein, we have studied the *in situ* reaction of 2-pyrimidinecarbonitrile with NH₂OH·HCl in the presence of Mn^{II} metal ions in methanolic medium at 60 °C to form the Mn(II) complex based on 2-pyrimidine amidooxime. This complex has also exhibited DNA binding activity, and this may appear as a potential activity for biomedical applications.

EXPERIMENTAL SECTION

Materials. The starting materials (Table 1) such as 2-pyrimidine carbonitrile, MnCl₂·4H₂O, NH₂OH·HCl, and NaOAc used for the preparation of complex were procured from Merck, India. Calf thymus DNA (sodium salt, D1501) and bisbenzimidazole (Hoechst 33258, ≥98% purity) were purchased from Sigma-Aldrich Corp. (St. Louis, MO, USA). All other solvents and chemicals were of reagent grade, obtained from commercial sources, and used without further purification.

Synthesis of the Complex [Mn^{II}(HL)₂(Cl)(CH₃COO)]-(1). [Mn^{II}(HL)₂(Cl)(CH₃COO)](1) was prepared by the following *in situ* preparation procedure (Scheme 1).³⁰ A mixture of 2-cyano pyrimidine (0.104 g, 1 mmol) and hydroxylamine hydrochloride (0.069 g, 1 mmol) in methanol (30 mL) was refluxed at 60 °C for 10 min to form pyrimidine 2-amidooxime (HL), and then, immediately MnCl₂·4H₂O (0.199 g, 1 mmol) was added to the hazy white solution and stirred for additional 25 min whereupon, the solution turned bright yellow. The stirring was continued for further 1 h with addition of NaOAc (0.082 g, 1 mmol) as a base, and the resulting solution was filtered and kept undisturbed, allowing slow evaporation for few days. The block-shaped yellowish single crystals were collected by filtration and washed with cold methanol. Anal. Calcd for C₁₂H₁₅ClMnN₈O₄ (MW 425.71 g/

mol): C, 33.86%; H, 3.55%; N, 26.32%. Found: C, 33.82%; H, 3.58%; N, 26.35%. IR (cm⁻¹, KBr): ν(-OH), 3027; ν(C=N), 1658; ν(CH₃COO⁻), 1426.

Physical Measurements. Elemental analyses (carbon, hydrogen, and nitrogen) of the metal complex were performed with a PerkinElmer CHN analyzer 2400. IR spectra (400–4000 cm⁻¹) were recorded on a Nicolet Magna IR 750 series-II FTIR spectrometer. UV–vis spectral titrations were carried out on a JASCO V660 spectrophotometer (JASCO, Hachioji, Japan). Fluorescence studies were performed on a Shimadzu RF-5301PC spectrofluorimeter (Shimadzu, Kyoto, Japan). A VP-ITC microcalorimeter (MicroCal, USA, now Malvern Instruments, UK) was used to perform isothermal titration calorimetry (ITC) experiments.

Crystallography. Single-crystal X-ray diffraction data of 1 were collected at 273(2) K on a quest diffractometer with graphite monochromated Mo K α radiation ($\lambda = 0.71073$ Å). Data integration and reduction were done by using the Bruker Smart Apex, data were integrated using the SAINT³¹ program, and the absorption corrections were made with SADABS.³² The structure was solved by direct methods,³³ and full-matrix least-squares refinements were performed on F^2 using SHELXL-2014/17 with anisotropic displacement parameters for all nonhydrogen atoms. All the nonhydrogen atoms were refined with anisotropic thermal parameters. All the hydrogen atoms belonging to carbon atoms were placed in their geometrically idealized positions. Molecular view and packing diagrams of complex 1 were produced with the Diamond Ver. 3.2 program.³⁴ The crystal data and details of refinement are given in Table 2.

Computational Details. The ground-state electronic structure calculation in the gas phase of 1 has been carried out using the density functional theory (DFT)³⁵ method

Table 2. Crystal Data and Structure Refinement for **1**

parameters	1
formula	C ₁₂ H ₁₅ ClMnN ₈ O ₄
formula Weight	425.71
crystal System	monoclinic
space group	P2 ₁ /c (no. 14)
a, b, c [Å]	13.1596(6), 15.2760(8), 8.7403(5)
α, β, γ [deg]	90, 108.474(2), 90
V [Å ³]	1666.48(15)
Z	4
D (calc) [g/cm ³]	1.697
μ (Mo Kα) [mm]	0.992
F(000)	868
crystal Size [mm]	0.18 × 0.29 × 0.35
temperature (K)	100
radiation [λ, Å]	0.71073
θ _{min} –max [deg]	2.7, 33.2
data set	–19: 19; –23: 23; –13: 13
tot., uniq. data, R _(int)	27324, 6324, 0.045
observed data [I > 2σ(I)]	5020
N _{ref} N _{par}	6324, 260
R, wR ₂ , S	0.0417, 0.1011, 1.05

associated with the conductor-like polarizable continuum model (CPCM).³⁶ Becke's hybrid function³⁷ with the Lee–Yang–Parr (LYP) correlation function³⁸ was used throughout the study. The absorbance spectral properties in dimethyl sulfoxide (DMSO) medium was calculated by time-dependent DFT (TDDFT)³⁹ associated with the CPCM. We computed the lowest 40 sextet–sextet transitions (as ligand environments of Mn(II) is in weak field strength, so the metal center is in high spin state with spin multiplicity 6 having the d⁵ system).

We employed 6-31+G** for C, H, N, O, Cl, and for Mn atoms, and we used LanL2DZ as the basis set for all the calculations. All the calculations were performed with the Gaussian 09W software package.⁴⁰ Gauss Sum 2.1 program⁴¹ was used to calculate the molecular orbital contributions from groups or atoms.

DNA Binding Measurements. DNA binding measurements were carried out following similar protocols elaborated previously.^{21,22,29,30} The DNA sample exhibited a characteristic ultraviolet absorption spectrum with an A₂₆₀/A₂₈₀ ratio between 1.88 and 1.92 and an A₂₆₀/A₂₃₀ ratio between 2.12 and 2.22. The DNA concentration in base pairs was estimated by recording absorbance at 260 nm employing a molar absorption coefficient (ε) value of 13,200 M^{–1} cm^{–1}. All experiments were performed in filtered 10 mM citrate–phosphate (CP) buffer, pH 7.0, prepared in triple-distilled water. Biophysical experiments were carried out in 2% DMSO–buffer (v/v) solution of the complex (**1**). The kinetic study of the decomposition of the complex in the 2% DMSO buffer (v/v) solution for 2.7 h was carried out to ascertain the stability of the complex **1** in the testing media.

Absorbance and Fluorescence Spectral Titrations. The absorption and fluorescence spectral titrations were performed at 298.15 ± 0.5 K using quartz cuvettes of path length 1 cm, following the methods standardized in our laboratory and reported earlier.^{21,22,29,30} The electronic spectra of **1** were monitored as a function of the concentration of DNA. In each case, a fixed concentration of **1** (20 μM) was titrated with increasing concentration of DNA (0–30 μM).

The steady-state fluorescence measurements were performed keeping the excitation wavelength for **1** at 350 nm with and excitation and emission band pass of 10 nm. Fixed concentration of **1** (20 μM) was titrated over the incremental concentration range of DNA (0–34 μM).

Estimation of the Binding Parameters. The binding affinity of **1** to DNA was estimated from absorbance and fluorescence titration data using modified Benesi–Hildebrand (BH) eq 1⁴²

$$\frac{1}{\Delta A} = \frac{1}{\Delta A_{\max}} + \frac{1}{(\Delta A_{\max})K_{\text{BH}}} \times \frac{1}{[M]} \quad (1)$$

Here, the difference in absorbance or fluorescence is denoted by ΔA, and [M] is the concentration of DNA. By plotting the reciprocal of the difference in absorbance/fluorescence intensity against the reciprocal of DNA concentration, the BH plot was constructed. The association constant (K_{BH}) for **1**–DNA complexation was calculated from the ratio of the intercept to the slope.^{21,22,30}

Continuous Variation Analysis (Job's Plot). Stoichiometry for the complexation of compound **1** with DNA was determined by the continuous variation method (Job's plot).⁴³ The fluorescence signal was recorded for solutions where the concentrations of both DNA and **1** were varied, while the sum of their concentrations was kept fixed. The plot of difference in fluorescence intensity (ΔF) of the compound at 430 nm was plotted as a function of the input mole fraction of **1**. Inflection point in the resulting plot corresponds to the mole fraction of the bound **1** in the DNA–**1** complex. The stoichiometry was obtained in terms of DNA–**1** [(1 – χ_{compound})/χ_{compound}], where, χ denotes the mole fraction of compound **1**. The results presented are average of three experiments.²¹

Determination of the Binding Mechanism by the Hoechst 33258 Displacement Assay. The competitive binding efficiency between Hoechst 33258 and **1** with DNA was determined by fluorimetry in the range of 400–600 nm.⁴⁴ Aliquots of stock solution of **1** (upto 0–32 μM) were added to the equilibrated mixture of CT–DNA (20 μM) and Hoechst 33258 (1.91 μM) (termed as the Hoechst–DNA complex) at room temperature. The excitation wavelength was set as 350 nm.

Circular Dichroism Spectral Study. Circular dichroism (CD) spectra were performed on a JASCO J815 model unit (JASCO International Co. Ltd. Japan) equipped with a JASCO temperature controller (PFD 425L/15) at 298.15 ± 0.5 K in the region 200–400 nm by following the literature methods.^{29,30} A rectangular stainless quartz cuvette of 1 cm path length was used. Titrations were performed by the addition of incremental concentrations of **1** to a fixed concentration of DNA (60 μM). The molar ellipticity values [θ] were calculated from the equation [θ] = 100 × θ/(C × l), where C is the concentration in moles/lit, and l is the cell path length of the cuvette in cm. The molar ellipticity [θ] (deg cm²/dmol) values are expressed in terms of base pairs.⁴³

Hydrodynamic Studies. Hydrodynamic studies were carried out to characterize the binding mode of the complex with DNA. The details of hydrodynamic studies are described in Supporting Information.

ITC Study. ITC studies were executed on a VP-ITC microcalorimeter to derive the binding and thermodynamic parameters of **1**–DNA association. During the titration, aliquots of **1** (128 μM) were injected from the rotating syringe into the isothermal chamber containing 60 μM, 1.4235 mL of DNA

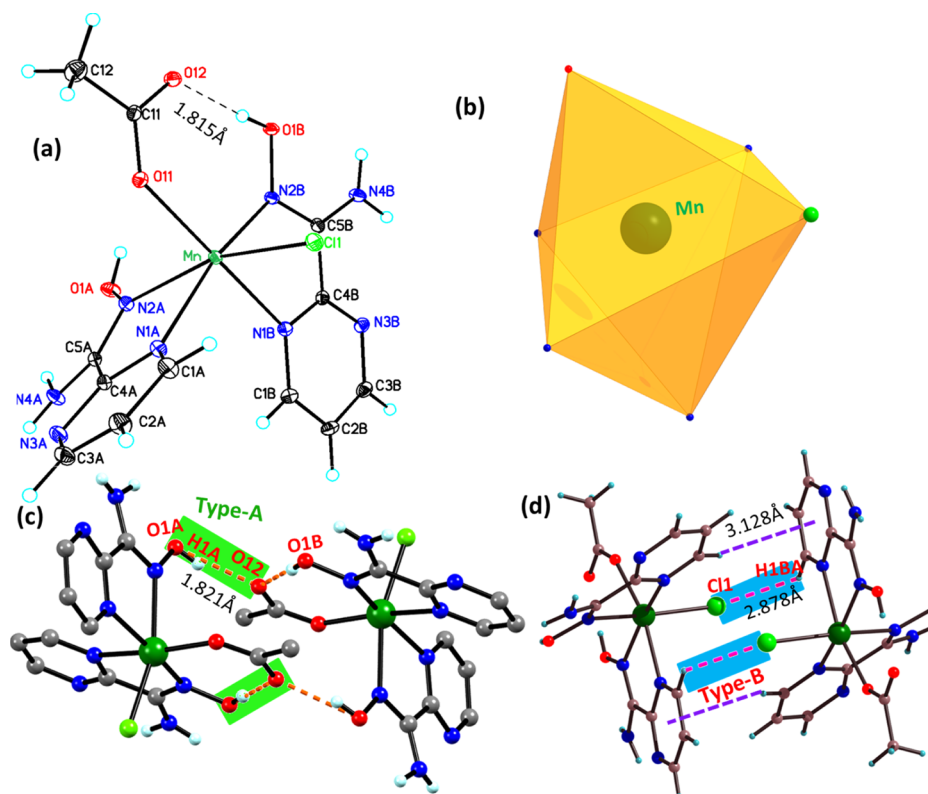


Figure 1. (a) ORTEP view (30% ellipsoid probability), (b) polyhedral representation of metal center, (c) supramolecular dimer formed by type-A intermolecular hydrogen-bonding interactions, (d) supramolecular dimer formed by type-B hydrogen-bonding interactions and by CH \cdots π interaction of **1**.

solutions maintained at 298.15 K. The titration was accomplished in 28 sequential injections, and each injection released 10 μ L aliquots from the syringe into the calorimeter cell. To avoid any bubble formation during the titration, the buffer solutions were degassed thoroughly. The heat accompanying each injection was noticed as a heat spike, which is eventually the quantity of the power needed to preserve the sample and reference cells at equal temperatures. The area under each peak was integrated to get the heat accompanying the injections. The corresponding dilution study was performed injecting same volumes of the identical concentration of **1** into the buffer alone in a separate experiment. The heats of dilution (control heats) were subtracted and the data fitted using the Origin software to a “one set of binding sites” model.^{29,30,43} The corrected injection heats were thereafter plotted as a function of the molar ratio to calculate the equilibrium constant (K), the binding stoichiometry (N), the standard molar enthalpy change (ΔH^0) of association, and standard molar entropy changes (ΔS^0). The standard molar Gibbs energy change (ΔG^0) was calculated using the standard relationship

$$\Delta G^0 = -RT \ln K$$

where R (1.9872036 cal K $^{-1}$ mol $^{-1}$) is the gas constant, and T is the temperature in Kelvins (K).

Molecular Docking Studies. To get explicit perception of the interaction and the mode of binding of **1** with CT-DNA, molecular docking simulations were carried out using the AutoDock 4.0 software package as accomplished by the graphical user interface AutoDock 4.0 (AD4.0-bound.dat). The macrocyclic receptor was chosen as the Protein Data Bank

(PDB) identifier 258D (GC content 33.33%) format of three-dimensional (3D) X-ray crystal structure of CT-DNA. The 3D structure of **1** was saved in a PDB format with the aid of the program Mercury 3.2. The graphical user interface AutoDock tools was devoted to set up the protein: the water molecule was deleted from the crystal of the protein, only polar hydrogen was added, computed Gasteiger charge was calculated as -25.9962 , and nonpolar hydrogen was merged to the carbon atom. Rotatable bonds of the complex molecules were identified with AutoDock tools. The AutoDock program was used to make the docking input file. Grid maps for **1** of $40 \times 44 \times 60$ Å with grid spacing of 1 Å were generated using the AutoGrid program. Both receptor and **1** were saved in the pdbqt format. A distance-dependent function of the dielectric constant was used for the calculation of the energetic map. Lamarckian genetic algorithm was used to carry out the docking calculations. Each run of the docking simulation was set to conclude after a maximum of 250,000 GA energy evaluations.⁴⁴ The optimized docked model with lowest docking energy was chosen for further analysis of docking simulations. The docked poses were analyzed and viewed in PyMOL software.

RESULTS AND DISCUSSION

Structural Description. The reaction of MnCl $_2$ ·6H $_2$ O (1 equiv) with the *in situ* formed amidooxime ligand (pyrimidine 2-carbonitrile and hydroxylamine hydrochloride in 1:1 ratio in methanol) and NaOAc (1 equiv) as the base in MeOH yielded the corresponding mononuclear Mn II complex **1**, the yellow single crystals of which were obtained by slow evaporation of the solvent.

The structural analyses from single-crystal X-ray diffraction studies show that complex **1** is a Mn^{II} mononuclear species that comprises one Mn^{II} ion, two dicoordinating N₂ donor-based 2-pyrimidine amidooxime ligands, and two one-terminal acetate (OAc⁻) ions and one-terminal Cl⁻ ions. It is crystallized in a *monoclinic* system with space group *P*₂₁/*c*. The structure consists of discrete [Mn^{II}(HL)₂(Cl)(CH₃COO)] as a neutral species in which the 2-pyrimidine amidooxime ligand is neutral, as shown in Figure 1a. It shows that the structure of [Mn^{II}(HL)₂(Cl)(CH₃COO)](**1**) is mononuclear in octahedral geometry surrounded by two neutral N₂ donor amidooxime ligands, occupying *cis* positions, while the two mono-negatively charged coligands (one chloride and one acetate) coordinated at the *cis* position to each other and satisfied the hexacoordination of the metal center. The Mn atom thus adopts distorted octahedral geometry being hexacoordinated with *cisoid* polyhedral shapes (Figure 1b). The bond lengths around the central Mn^{II} ion are Mn–N1A(pyrimidine-N) = 2.289(1) Å, Mn–N1B(pyrimidine-N) = 2.323(1) Å, Mn–N2A(oximate) = 2.328(2) Å, Mn–N2B(oximate) = 2.224(1) Å, Mn–O11(acetate) = 2.116(1) Å, and Mn–Cl1(chloro) = 2.461(5) Å. The selected bond lengths and bond angles are given in Table 3; these agreed well with the normal reported values in

Table 3. Selected Bond Distances and Bond Angles of **1**

bond type	bond length (Å)	bond type	bond angles (deg)
Mn–Cl1	2.4613(5)	O11–Mn–N2A	89.43(5)
Mn–O11	2.1158(11)	O11–Mn–N2B	100.55(5)
Mn–N1A	2.2892(14)	N1A–Mn–N1B	94.28(5)
Mn–N1B	2.3226(13)	N1A–Mn–N2A	70.15(5)
Mn–N2A	2.3280(15)	N1A–Mn–N2B	164.22(5)
Mn–N2B	2.2243(14)	N1B–Mn–N2A	83.29(5)
bond angles (deg)		N1B–Mn–N2B	71.13(5)
Cl1–Mn–O11	97.45(4)	N2A–Mn–N2B	101.34(5)
Cl1–Mn–N1A	91.91(4)	O11–Mn–N1A	92.79(5)
Cl1–Mn–N1B	92.62(4)	O11–Mn–N1B	167.49(5)
Cl1–Mn–N2A	161.15(4)	Cl1–Mn–N2B	94.66(4)

analogous Mn^{II} complexes.³⁰ The Mn^{II}–Mn^{II} intermolecular distance is 6.729 Å. The dihedral angle between two well-defined planes around Mn (Mn N1B N2B O11N1A) and (Mn N1A N2A N2B Cl1) is 89.76°. The mean deviation of these two intersecting perpendicular planes is 0.000 Å. The intramolecular H-bonds are between oxime-OH (O1B) and acetate-O(O12); O1B–H1B[⋯]O12 = 1.815 Å. The bond valence sum calculation results are shown in Table S1, where it can be seen that the oxidation state of manganese is 2.020 (~2). Thus, the central metal atom Mn is in a +2 oxidation state.

Inspection of molecular assemblies through supramolecular interactions shows that **1** forms two types (A and B) of supramolecular dimers. Type A: the intermolecular H-bonding is between oxime-OH(O1A) and acetate-O(O12); O1A–H1A[⋯]O12 = 1.821 Å (Figure 1c) and type B: the intermolecular H-bonding is between the pyrimidine ring C–H atom (H1BA) and chlorine atom (Cl1); C1B–H1BA[⋯]Cl1 = 2.878 Å and noncovalent CH[⋯]π interaction (3.128 Å) (Figure 1d) between H atom (H1AA) of one pyrimidine ring and the centroid of the neighboring pyrimidine ring. The dimer type A is extended in an one-dimensional (1D) network

(Figure 2a) through intermolecular hydrogen-bonding interactions (Table S2) (between amido H atom (H4B2 and H4A2) with oximate-O(O1B) and acetate-O(O11): N4B–H4B2[⋯]O1B = 2.921 Å and N4A–H4A2[⋯]O11 = 2.162 Å interactions) along the crystallographic *b* axis. This 1D supramolecular assembly is further extended to the two-dimensional (2D) framework in the crystallographic *bc* plane (Figure 2b).

The dimer type B is also extended in a 1D framework (Figure S1) through intermolecular hydrogen-bonding interactions [between the pyrimidine ring C–H atom (H2BA) and chlorine atom (Cl1); C2B–H2BA[⋯]Cl1 = 2.905 Å] along the crystallographic *c* axis. The close packing interaction exhibits that the supramolecular 2D structure is expanded to form a 3D network along the crystallographic *a* axis (Figure 2c).

Geometry Optimization and Electronic Structure. The geometry of complex **1** was optimized in the ground state. The optimized geometry of **1** is comparable with the molecular structure from single-crystal X-ray diffraction (SCXRD) in Figure 3. The energy difference between highest occupied molecular orbital (HOMO) and lowest unoccupied molecular orbital (LUMO) is 3.61 eV (Figure 3a). The Frontier molecular orbital (FMO) diagram with the respective positive and negative regions of the optimization of **1** is shown in Figure 3. The positive and negative phases are represented in green and blue, respectively.

The electronic spectrum of **1** in DMSO (2 × 10⁻⁵ (M)) solution shows a band at 283 nm (ε = 1.75 × 10⁴ M⁻¹ cm⁻¹). This is attributed to ligand-to-metal charge transfer transition (LMCT). The experimentally observed absorption bands of the complex have been explained with the help of TD-DFT calculations in application of the CPCM model assuming Mn(II) is in high spin state having a spin multiplicity of 6. The theoretical bond lengths in the gas phase are compared with crystallographic bond distances (Table S3).

The absorption spectra of **1** were studied at room temperature in DMSO. The complex (**1**) shows a well-resolved absorption band located at 298.36 nm, having LMCT, which is in good agreement with the experimental result of 283 nm. This absorption band can be assigned to the S₀ → S₄₀ electronic transition (Table 4) with an oscillator strength *f* = 0.0066 (Figure 3b).

DNA Binding Studies. Absorbance Spectral Studies. UV–visible absorption spectroscopy is one of the most used methods for studying the binding interaction of small molecules with DNA. Usually, when a molecule or compound binds with the DNA helix, variations in the absorbance maxima and/or the shift in the peak position are observed.^{45–48} The efficacy of interaction is associated with the extent of changes or shifting of the peak position in the absorbance spectra. The electronic absorption of **1** at 283 nm was monitored in the presence and absence of DNA which showed 54% hyperchromism and 4 nm red shift upon incremental addition of DNA (Figure 4). Such spectral observation may be ascribed to an effective interaction among the DNA base pairs with the π electron clouds of the interacting moiety.⁴⁹ Binding data collected from the absorbance titration were used to construct the BH plot to evaluate the apparent equilibrium constant (K_{BH}). From spectrophotometry, the magnitude of apparent equilibrium constant (K_{BH}) for **1**–DNA complexation was deduced to be (3.67 ± 0.04) × 10⁵ M⁻¹ (Table 5). Again, the kinetic studies of the decomposition of the complex exhibited

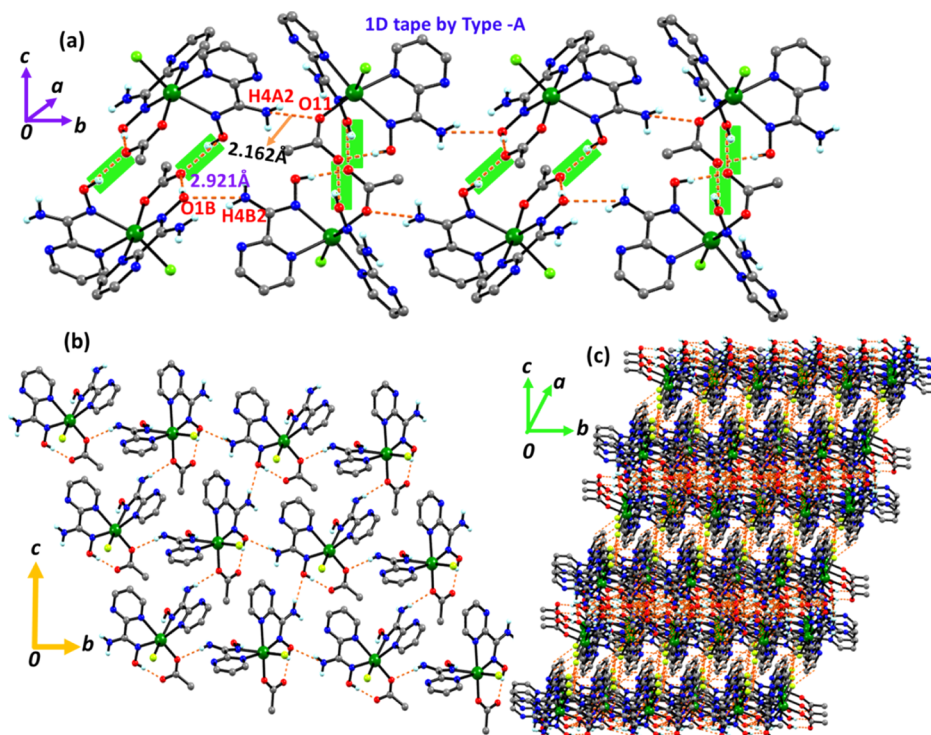


Figure 2. (a) Supramolecular 1D network through the type A intermolecular hydrogen-bonding interactions; (b) extended 2D supramolecular framework in the crystallographic *bc* plane; (c) close packing diagram of the 3D framework along the crystallographic *a* axis of **1**.

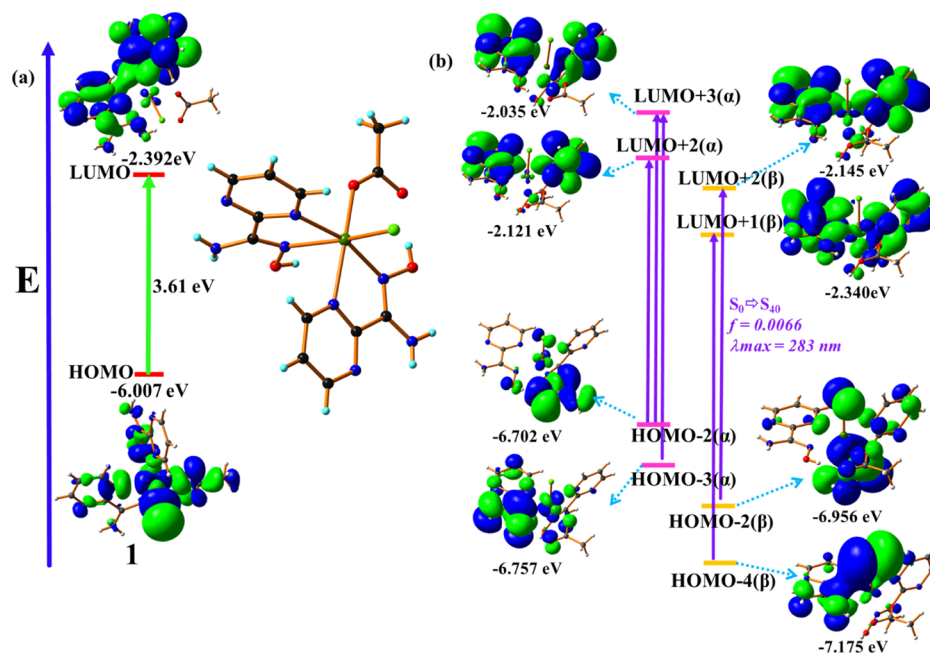


Figure 3. (a) FMOs (left) and optimized geometry (right) of **1**, (b) FMOs involved in the UV-vis absorption of **1** in DMSO solution.

Table 4. Comparable Calculated Absorbance λ_{max} with Experimental Values for **1**

theoretical (nm)	experimental (nm)	composition	CI	transition	energy (eV)	<i>f</i>
298.36	283	HOMO - 2(α) → LUMO + 3(α)	0.13323	$S_0 \rightarrow S_{40}$	4.1556	0.0066
		HOMO - 2(α) → LUMO + 2(α)	0.17607			
		HOMO - 3(α) → LUMO + 3(α)	0.14466			
		HOMO - 2(β) → LUMO + 2(β)	0.31646			
		HOMO - 4(β) → LUMO + 1(β)	0.19340			

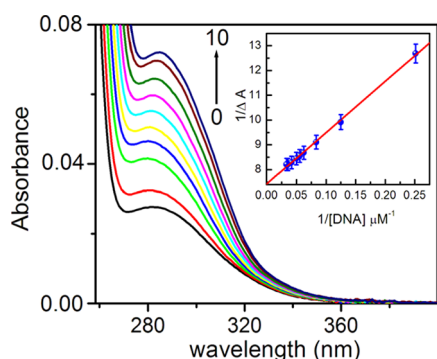


Figure 4. Absorbance titration profile of **1** (20 μM) in the presence of increasing concentration of DNA [0–30 μM]; inset: modified BH plot.

that complex **1** shows sufficient stability in the testing media ($t_{1/2} \sim 15$ h) (Figure S2).

Steady-State Fluorescence Titration. The complex (**1**) exhibited an emission maximum at 430 nm when excited at 350 nm. The steady-state fluorescence titration was carried out by a fixed concentration of **1** (20 μM) with incremental addition of DNA. About 10-fold enhancement in the emission intensity of **1** was observed without any appreciable shift in the emission maximum (Figure 5). This increase in the emission intensity upon binding to DNA indicates a significant interaction of compound **1** with DNA. From BH plot, the binding affinity (K_{BH}) was estimated as $(4.10 \pm 0.04) \times 10^5 \text{ M}^{-1}$ (Table 5).

CD Spectral Study. The effect of **1** on the conformation of DNA was further investigated by CD spectroscopy. CD spectrum of CT DNA displayed a classical B-form conformation with a large positive band around 270–280 nm, a negative band at 248 nm, and a small positive band in the 210–220 nm regions (Figure 6). In the presence of the manganese compound **1**, only a lessening of the molar ellipticity of the DNA bands was observed, indicating that **1** binds to DNA with retention of the actual B-conformation of free DNA.^{29,30}

Continuous Variation Analysis (Job's Plot). The continuous variation protocol (Job plot) was used to estimate the binding stoichiometry of **1** in the **1**-DNA complexation.²¹ The plot of fluorescence intensity difference (ΔF) at λ_{max} versus the mole fraction of **1** revealed a single binding mode. From the inflection point, χ value was found to be 0.512, from which the stoichiometry was estimated to be around 0.95 (Figure 7).

Determination of the Binding Mechanism by the Hoechst 33258 Displacement Assay. A synthetic *N*-methylpiperazine analogue Hoechst 33258 displays a precise binding affinity for the A-T rich sequences at the minor

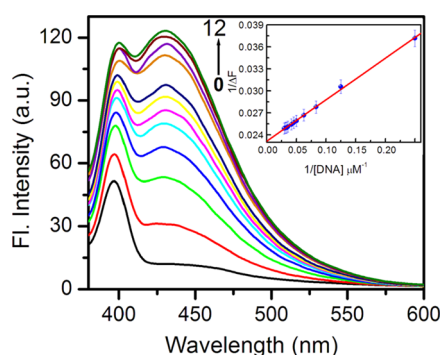


Figure 5. Steady-state fluorescence titration of **1** (20 μM) with DNA [0–34 μM]; $\lambda_{\text{excitation}} = 350$ nm; inset: modified B–H plot.

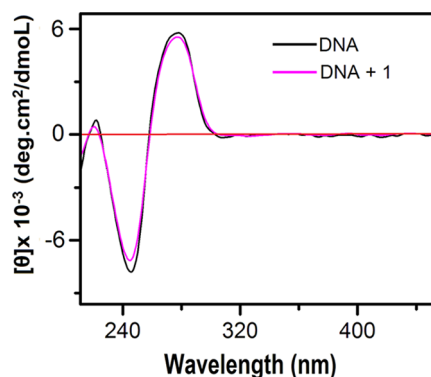


Figure 6. CD spectral profile of DNA (60 μM) on addition of **1** (40 μM) in 10 mM CP buffer.

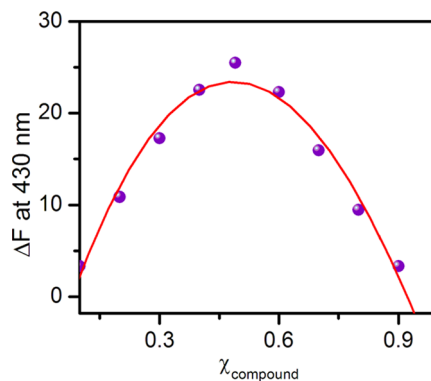


Figure 7. Job's plot for depicting the change in fluorescence intensity vs mole fraction of **1**.

grooves of DNA. For investigation the binding site of **1** in the DNA helix, the Hoechst displacement assay was carried out. In the presence of DNA, a sharp increase in the emission intensity

Table 5. Binding Parameters for the Association of DNA with Oxime-Based Mn Complexes^a

complexes	spectrophotometry K_i (M^{-1})	spectrofluorimetry K_i (M^{-1})	binding Mode	refs
$[\text{Mn}(\text{HL}_1)_2](\text{Cl})_2$	2.18×10^5	2.22×10^5	partial intercalation	30
$[\text{Mn}(\text{HL}_1)_2](\text{Cl})(\text{N}_3)$	1.79×10^5	1.56×10^5	"	30
$[\text{Mn}(\text{HL}_2)_2](\text{Cl})_2$	2.05×10^4	2.97×10^4	"	30
$[\text{Mn}(\text{HL}_2)_2](\text{Cl})(\text{N}_3)$	1.52×10^4	1.61×10^4	"	30
$[\text{Mn}_3\text{O}(\text{S-Br-salox})_3(\text{NO}_3)(\text{H}_2\text{O})_4]$	1.63×10^6	1.59×10^6	minor groove	29
$[\text{Mn}^{\text{II}}(\text{HL}_1)_2(\text{Cl})(\text{CH}_3\text{COO})]$	3.67×10^5	4.10×10^5	minor groove	this work

^aHL₁ = pyrimidine amidooxime, HL₂ = pyridine amidooxime.

of Hoechst is observed, which is due to the greater planarity of the *N*-methylpiperazine moiety of Hoechst when bound to double-stranded DNA and its protection from collisional quenching.⁵⁰ If **1** competes for the similar DNA binding sites of Hoechst, a reduction of the fluorescence intensity of the latter must be detected. As depicted in Figure 8, the

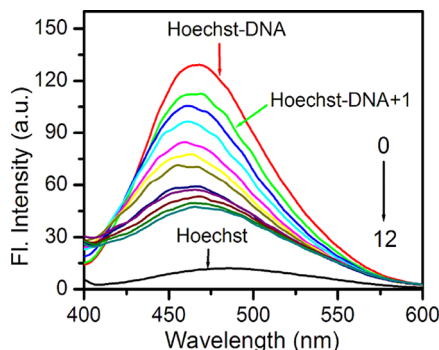


Figure 8. Fluorescence emission spectra of the competition between the Hoechst–DNA complex (λ_{exc} : 350 nm) and **1**. $C_{\text{Hoechst}} = 1.91 \mu\text{M}$ and $C_{\text{DNA}} = 20 \mu\text{M}$, C_1 : 0.0–32 μM . Inset: plot of relative quenching of Hoechst–DNA complex by **1**.

fluorescence of the Hoechst–DNA complex was reduced (~70%) by the addition of **1**. Figure 9 represents the Stern–

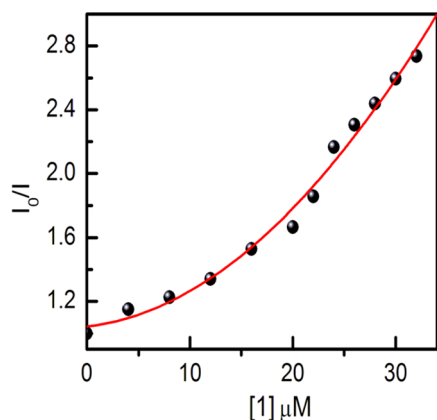


Figure 9. Stern–Volmer plot for the fluorescence quenching of the Hoechst–DNA complex system by **1**.

Volmer plot for the fluorescence quenching of the Hoechst–DNA system by **1**. This observation suggests that **1** can dislocate Hoechst essentially from the adenine- and thymine-binding sites in the minor groove of DNA.^{29,30,44}

Hydrodynamic Studies. Hydrodynamic study is an important method for ascertaining the mode of binding of small molecules with DNA. During intercalation, the axial length and rigidity of the helical duplex increases. Both factors enhance the frictional coefficient and the viscosity of DNA in solution.²¹ On the other hand, the effective length of DNA decreases in case of surface or groove binding, leading to a minor decrease in the relative viscosity of the DNA solution. The viscosity of the DNA solution was estimated in the presence of increasing concentrations of **1** (Figure S3). Only marginal change was found in the relative viscosity of DNA in the presence of **1**. Such minor changes in relative viscosity may be associated to a groove binding model.²⁹

ITC Studies. ITC is an extremely sensitive and reliable technique for investigation of the binding parameters when a molecule forms complex with DNA. A single ITC experiment can yield all values of thermodynamic parameters such as equilibrium constant (K), stoichiometry (N), standard molar Gibbs energy change (ΔG^0), standard molar enthalpy change (ΔH^0), and entropic contribution ($T\Delta S^0$) to the binding.^{21,29,43} In order to get an in-depth knowledge on the binding of **1** to DNA, ITC study was performed.²⁹ Figure 10

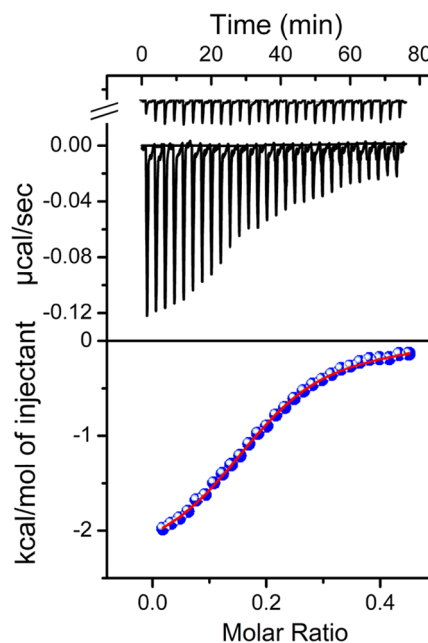


Figure 10. ITC profile **1**-DNA interaction at $T = 298.15 \text{ K}$. The top panel represents the raw data resulting from the sequential injection of **1** (128 μM) into 60 μM DNA solution. The first series of peaks in the top panel are the control heats, that is, dilution heats for injecting identical volumes of the same concentration of the **1** into the buffer. The lower panel represents the corresponding normalized heat signals vs molar ratio. The data points (●) are the experimental injection heats, while the continuous line is the best fit curve using a single-binding site model.

depicts the calorimetric profile for the titration of **1** into the DNA solution at 298.15 K. The thermogram reveals exothermic interaction with one binding event. The binding constant was deduced to be $(4.39 \pm 0.01) \times 10^5 \text{ M}^{-1}$, which is in close agreement with the binding constant values obtained from spectroscopic analysis. The stoichiometry value (N) was found to be 0.193. The site size value (n) is defined as the reciprocal of the stoichiometry value (N). Here, the value of n comes out to be 5.18. The standard enthalpy value as determined from ITC is $-2.45 \text{ kcal mol}^{-1}$. The thermodynamic parameters clearly indicate that the interaction of **1** with DNA was favored by small negative enthalpy ($\Delta H^0 = -2.45 \text{ kcal mol}^{-1}$) and large positive entropy ($T\Delta S^0 = 5.25 \text{ kcal mol}^{-1}$) changes. Therefore, it can be concluded that the binding process is entropy-driven.²¹ The thermodynamic parameters are enlisted in Table 6.

Molecular Docking Studies. Molecular docking simulations have now appeared as an emerging tool in drug discovery for showing the binding mode and interaction between small molecules as the complex and DNA.²³ The docked conformations of **1** with CT–DNA are displayed in

Table 6. Thermodynamic Parameters for the Association of 1 with CT-DNA at 298.15 K

compound	10^{-5} K/M^{-1}	$\Delta H^0/\text{kcal mol}^{-1}$	$T\Delta S^0/\text{kcal mol}^{-1}$	$\Delta G^0/\text{kcal mol}^{-1}$
1	4.39 ± 0.01	-2.45 ± 0.01	5.25 ± 0.01	-7.70 ± 0.05

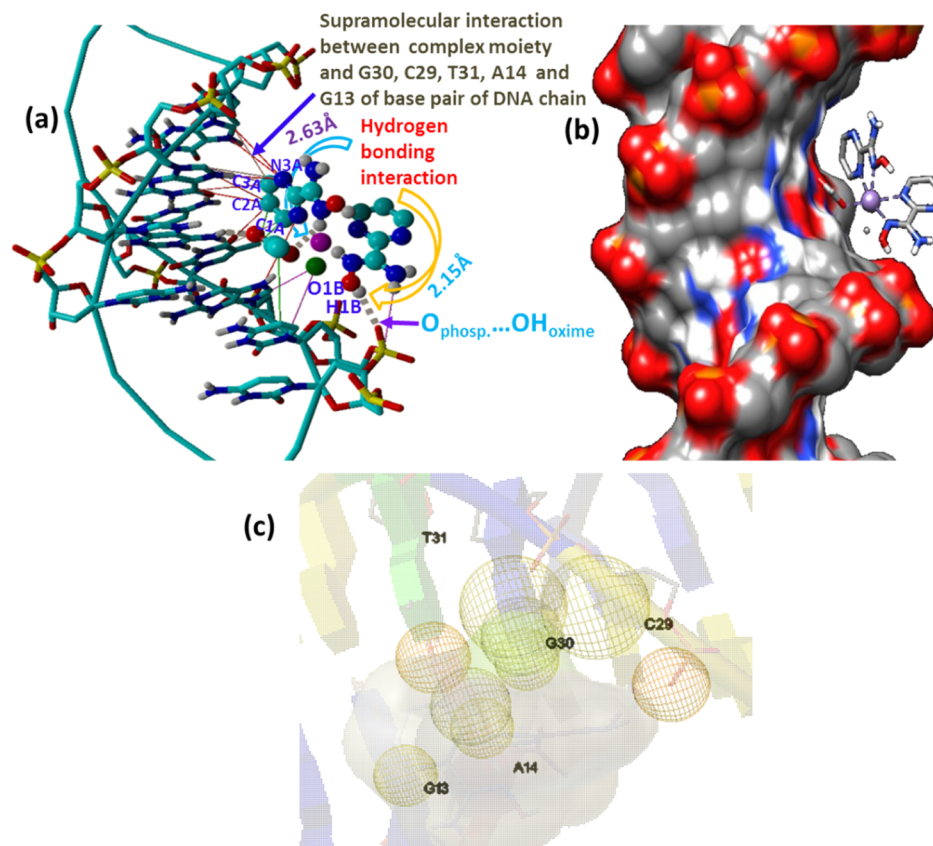


Figure 11. (a) Capped-ball and stick model viewed into the minor groove of DNA with 1. The important interactions between different sections of the 1-DNA complex are illustrated with a red solid line and by gray dashed lines. The noncoordinated oxime-OH group forms strong hydrogen bonds with the phosphate-O; they are colored sky blue, white, red, blue, yellow, magenta, and green (C, H, O, N, P, Mn, and Cl, respectively); (b) space-filled model of the binding mode and hydrophobic interaction of 1 with DNA; (c) DNA is shown in surface; the interactions are shown in the solid surface with 50% transparency.

Table 7. Parameters from Molecular Docking Studies for DNA-1 Interaction

complex	complex-PDB	DNA-PDB source	simulation energies kcal mol^{-1}	atoms involvement (DNA)	mode of interaction
1	CIF file from SCXRD (CCDC no-2000190)	258D (GC content 33.33%) format	free binding energy = -6.66 intermolecular energy = -13.65 electrostatic energy = -2.25 free torsional energy = $+4.79$	G30, C29, T31, A14, G13 and phosphate linkage	minor Groove

Figure 11. It can be observed that the complex is well fitted in the active side of the DNA, which corroborates well with the experimental binding parameters obtained from ITC measurements and with docking studies. The favorable calculated free binding energy of 1 with DNA is -6.66 kcal/mol, and the final intermolecular energy is -13.65 kcal/mol (vdW + H-bond + desolvation energy = -13.01 kcal/mol). Other energies which are related for calculating the binding modes (Table 7), that is, electrostatic energy = -2.25 kcal/mol; free torsional energy = $+4.79$ kcal/mol. The complex shows supramolecular interaction with G30, C29, T31, A14, and G13 base pairs of the DNA chain and hydrogen bonding interactions between

oxime-OH and oxygen of phosphate linkages (Figure 11a). The complex also exhibits hydrophobic interactions with base pairs of the DNA chain (Figure 11b). Docking study reveals that interaction of the said compound with DNA is energetically the most favorable binding mode, and the surface model is shown in Figure 11c. This induces some additional steric hindrance to the moiety of 1 affecting the minor groove binding and the binding energy. Thus, the molecular docking study explained the different binding modes and binding affinities theoretically, which are consistent with the experimental observations.

CONCLUSIONS

The octahedral mononuclear Mn(II) complex based on the amidooxime ligand was synthesized by the reaction between cyanopyrimidine and hydroxylamine hydrochloride in the presence of Mn(II) ions and NaOAc. The structural characterization is done by single-crystal X-ray crystallography and compared with theoretical optimization using DFT/B3LYP. The interaction of the compound with CT-DNA was studied and confirmed by spectroscopic (viz: UV-vis, fluorometry, and CD), hydrodynamic, and calorimetric techniques which showed that **1** binds with CT-DNA through the groove binding mode. Hoechst displacement studies further confirmed that **1** interacts with double stranded DNA at the adenine and thymine (A-T)-binding sites located in the minor groove. From the thermodynamics study, the binding constant was estimated to be $(4.39 \pm 0.01) \times 10^5 \text{ M}^{-1}$. The calorimetric technique further confirms the spontaneity of the binding of **1** with DNA through an entropically driven interaction. Thus, this complex may be employed as a DNA targeted probe in the near future after physiological study and toxicity measurements. Molecular docking study also revealed that **1** is a minor groove binder toward DNA.

ASSOCIATED CONTENT

Supporting Information

The Supporting Information is available free of charge at <https://pubs.acs.org/doi/10.1021/acs.jced.0c00529>.

CCDC 2000190 containing the supplementary crystallographic data for **1**; and Protein Data Bank (PDB) identifier 258D (GC content 33.33%) format of the 3D X-ray crystal structure of CT-DNA obtained from biological macromolecular structures enabling breakthroughs in research and education (PDF)

AUTHOR INFORMATION

Corresponding Author

Malay Dolai – Department of Chemistry, Prabhat Kumar College, Purba Medinipur 721404, West Bengal, India; orcid.org/0000-0001-7697-3376; Email: dolaimalay@yahoo.in

Authors

Urmila Saha – Organic and Medicinal Chemistry Division, CSIR-Indian Institute of Chemical Biology, Kolkata 700 032, India

Gopinatha Suresh Kumar – Organic and Medicinal Chemistry Division, CSIR-Indian Institute of Chemical Biology, Kolkata 700 032, India; orcid.org/0000-0002-3596-979X

Ray J. Butcher – Department of Chemistry, Howard University, Washington, D.C. 20059, United States

Saugata Konar – Department of Chemistry, The Bhawanipur Education Society College, Kolkata 700020, India; orcid.org/0000-0001-5404-9107

Complete contact information is available at: <https://pubs.acs.org/doi/10.1021/acs.jced.0c00529>

Notes

The authors declare no competing financial interest.

ACKNOWLEDGMENTS

We gratefully acknowledge the Science & Engineering Research Board (SERB), Govt. of India, for the award of the

National Post-Doctoral Fellowship to the US (ref. no. PDF/2016/000080) and M.D. (ref. no. PDF/2016/000334). M.D. thanks Pradip Bera, Department of Chemistry, Kandi Raj College, Murshidabad, West Bengal, India, for his help in molecular docking studies. G.S.K. acknowledges financial support by the Council of Scientific and Industrial Research (CSIR), Govt. of India, to his laboratory through the Net Work Project “BIOCERAM” (ESC 0103).

REFERENCES

- (1) Banu, K. S.; Chattopadhyay, T.; Banerjee, A.; Mukherjee, M.; Bhattacharya, S.; Patra, G. K.; Zangrando, E.; Das, D. Mono- and dinuclear manganese(III) complexes showing efficient catechol oxidase activity: syntheses, characterization and spectroscopic studies. *Dalton Trans.* **2009**, 8755–8764.
- (2) Borgstahi, G. E.; Parge, H. E.; Hickey, M. J.; Beyer, W. F.; Hallewell, R. A.; Tainer, J. A. The structure of human mitochondrial manganese superoxide dismutase reveals a novel tetrameric interface of two 4-helix bundles. *Cell* **1992**, *71*, 107–118.
- (3) Pitie, M.; Boldron, C.; Pratviel, G. DNA Oxidation by Copper and Manganese Complexes. *Advances in Inorganic Chemistry*; Eldik, R., Reedijk, J., Eds.; Elsevier: Amsterdam, 2006; Vol. 58, pp 77–130.
- (4) Li, M. X.; Chen, C. L.; Zhang, D.; Niu, J. Y.; Ji, B. S. Mn(II), Co(II) and Zn(II) complexes with heterocyclic substituted thiosemicarbazones: synthesis, characterization, X-ray crystal structures and antitumor comparison. *Eur. J. Med. Chem* **2010**, *45*, 3169–3177.
- (5) Qiu-Yun, C.; Dong-Fang, Z.; Juan, H.; Wen-Jie, G.; Jing, G. Synthesis, anticancer activities, interaction with DNA and mitochondria of manganese complexes. *J. Inorg. Biochem.* **2010**, *104*, 1141–1147.
- (6) Abdel-Rahman, L. H.; Abu-Dief, A. M.; Hassan Abdel-Mawgoud, A. A. Development, structural investigation, DNA binding, antimicrobial screening and anticancer activities of two novel quaridentate VO (II) and Mn (II) mononuclear complexes. *J. King Saud Univ., Sci.* **2019**, *31*, 52–60.
- (7) Singh, D. P.; Kumar, K.; Sharma, C. New 14-membered octaazamacrocyclic complexes: Synthesis, spectral, antibacterial and antifungal studies. *Eur. J. Med. Chem.* **2010**, *45*, 1230–1236.
- (8) Sakiyan, I.; Logoglu, E.; Arslan, S.; Sari, N.; Sakiyan, N. Antimicrobial activities of N-(2-hydroxy-1-naphthalidene)-amino acid(glycine, alanine, phenylalanine, histidine, tryptophane) Schiff bases and their manganese(III) complexes. *BioMetals* **2004**, *17*, 115–120.
- (9) Abdel-Rahman, L. H.; Ismail, N. M.; Ismael, M.; Abu-Dief, A. M.; Ahmed, E. A.-H. Synthesis, characterization, DFT calculations and biological studies of Mn(II), Fe(II), Co(II) and Cd(II) complexes based on a tetradentate ONNO donor Schiff base ligand. *J. Mol. Struct.* **2017**, *1134*, 851–862.
- (10) Balakrishnan, M.; Kochukittan, M. Synthesis, characterization and antibacterial properties of some trivalent metal complexes with [(2-hydroxy-1-naphthaldehyde)-3-isatin]-bis hydrazone. *J. Enzyme Inhib. Med. Chem.* **2007**, *22*, 65–70.
- (11) El Mchichi, B.; Hadji, A.; Vazquez, A.; Leca, G. p38 MAPK and MSK1 mediate caspase-8 activation in manganese-induced mitochondria-dependent cell death. *Cell Death Differ.* **2007**, *14*, 1826–1836.
- (12) Oubrahim, H.; Stadtman, E. R.; Chock, P. B. Mitochondria play no roles in Mn(II)-induced apoptosis in HeLa cells. *Proc. Natl. Acad. Sci. U.S.A.* **2001**, *98*, 9505–9510.
- (13) Kovala-Demertzi, D.; Hadjipavlou-Litina, D.; Staninska, M.; Primikiri, A.; Kotoglou, C.; Demertzis, M. A. Anti-oxidant, in vitro, in vivo anti-inflammatory activity and antiproliferative activity of mefenamic acid and its metal complexes with manganese(II), cobalt(II), nickel(II), copper(II) and zinc(II). *J. Enzyme Inhib. Med. Chem.* **2009**, *24*, 742–752.
- (14) Kulaksizoglu, S.; Gökçe, C.; Gup, R. Structural variations and formation constants of first-row transition metal complexes of

biologically active aroylhydrazones. *Eur. J. Inorg. Chem.* **2003**, 1145–1156.

(15) Zhang, Q.; Huang, Y.; Guo, L.; Chen, C.; Guo, D.; Chen, Y.; Fu, Y. DNA-based nanocomposite as electrochemical chiral sensing platform for the enantioselective interaction with quinine and quinidine. *New J. Chem.* **2014**, *38*, 4600–4606.

(16) Saha, U.; Dolai, M.; Suresh Kumar, G. Adaptable Sensor for Employing Fluorometric Detection of Methanol Molecules: Theoretical Aspects and DNA Binding Studies. *New J. Chem.* **2019**, *43*, 8982–8992.

(17) Abu-Dief, A. M.; Alsehli, M. DNA Interaction of Drug Molecules for Cancer Treatment. *J. Pharm. Nurs.* **2019**, *2*, 12–16.

(18) Abdel-Rahman, L. H.; Abdelhamid, A. A.; Abu-Dief, A. M.; Shehata, M. R.; Bakheet, M. A. Facile synthesis, X-Ray structure of new multi-substituted aryl imidazole ligand, biological screening and DNA binding of its Cr(III), Fe(III) and Cu(II) coordination compounds as potential antibiotic and anticancer drugs. *J. Mol. Struct.* **2020**, *1200*, 127034–127045.

(19) Abdel-Rahman, L. H.; Abu-Dief, A. M.; Moustafa, H.; Hamdan, S. K. Ni(II) and Cu(II) complexes with ONNO asymmetric tetradentate Schiff base ligand: synthesis, spectroscopic characterization, theoretical calculations, DNA interaction and antimicrobial studies. *Appl. Organomet. Chem.* **2017**, *31*, No. e3555.

(20) Abdel-Rahman, L. H.; Abu-Dief, A. M.; El-Khatib, R. M.; Abdel-Fatah, S. M. Sonochemical synthesis, DNA binding, antimicrobial evaluation and in vitro anticancer activity of three new nano-sized Cu(II), Co(II) and Ni(II) chelates based on tridentate NOO imine ligands as precursors for metal oxides. *J. Photochem. Photobiol., B* **2016**, *162*, 298–308.

(21) Saha, U.; Dolai, M.; Kumar, G. S. Targeting nucleic acid with a bioactive fluorophore: Insights from spectroscopic and calorimetric studies. *J. Mol. Struct.* **2020**, *1220*, 128690–128696.

(22) Chakraborty, I.; Saha, U.; Rakshit, R.; Talukdar, S.; Kumar, G. S.; Mandal, K. Design and development of bioactive α -hydroxycarboxylate group modified MnFe₂O₄ nanoparticle: Comparative fluorescence study, magnetism and DNA nuclease activity. *Mater. Today Chem.* **2017**, *5*, 92–100.

(23) Zhao, Z.; Zhang, J.; Zhi, S.; Song, W.; Zhao, J. a. Novel binuclear and trinuclear metal (II) complexes: DNA interactions and in vitro anticancer activity through apoptosis. *J. Inorg. Biochem.* **2019**, *197*, 110696–110705.

(24) Inclán, M.; Albelda, M. T.; Frías, J. C.; Blasco, S.; Verdejo, B.; Serena, C.; Serena, C.; Salat-Canela, M. L.; García-España, A.; García-España, E. Modulation of DNA binding by reversible metal-controlled molecular reorganizations of Scorpion-like ligands. *J. Am. Chem. Soc.* **2012**, *134*, 9644–9656.

(25) van Rijt, S. H.; Sadler, P. J. Current applications and future potential for bioinorganic chemistry in the development of anticancer drugs. *Drug Discovery Today* **2009**, *14*, 1089–1097.

(26) Hernandez, M. Z.; de, S.; Pontes, F. J.; Coelho, L. C.; Moreira, D. R.; Pereira, V. R.; Leite, A. C. Recent insights on the medicinal chemistry of metal-based compounds: Hints for the successful drug design. *Curr. Med. Chem.* **2010**, *17*, 3739–3750.

(27) Kumar, C. V.; Asuncion, E. H. DNA Binding Studies and Site Selective Fluorescence Sensitization of an Anthryl Probe. *J. Am. Chem. Soc.* **1993**, *115*, 8547–8553.

(28) Børresen, H. C.; Grønbaek, R.; Mandell, L.; Kvande, P. C.; Meisingseth, E. On the luminescence properties of some purines and pyrimidines. *Acta Chem. Scand.* **1963**, *17*, 921–929.

(29) Dolai, M.; Saha, U.; Suresh Kumar, G.; Zangrando, E.; Ali, M. Synthesis, Structure and DNA Binding Studies of Oxime Based [Mn₃(μ_3 -O)]⁷⁺ complex. *Inorg. Chim. Acta* **2018**, *483*, 211–217.

(30) Dolai, M.; Saha, U.; Kumar, G. S.; Ali, M. Amidoxime-Based Mononuclear Mn (II) Complexes: Synthesis, Characterization, and Studies on DNA Binding and Nuclease Activity. *ChemistrySelect* **2018**, *3*, 6935–6941.

(31) SMART (V 5.628), SAINT (V 6.45a), XPREP, SHELXTL; Bruker AXS Inc.: Madison, WI, 2004; p 2004.

(32) Altomare, A.; Burla, M. C.; Camalli, M.; Cascarano, G. L.; Giacovazzo, C.; Guagliardi, A.; Moliterni, A. G. G.; Polidori, G.; Spagna, R. SIR97: a new tool for crystal structure determination and refinement. *J. Appl. Crystallogr.* **1999**, *32*, 115–119.

(33) Sheldrick, G. M. Crystal structure refinement with SHELXL. *Acta Crystallogr., Sect. C: Struct. Chem.* **2015**, *71*, 3–8.

(34) Brandenburg, K. [or Brandenburg, K. & Putz, H., or Brandenburg, K. & Berndt, M.]. DIAMOND; Crystal Impact GbR: Bonn, Germany, 1999.

(35) Parr, R. G. Density-Functional Theory of Atoms and Molecules. *Horiz. Quant. Chem.* **1980**, *3*, 5–15.

(36) Cossi, M.; Rega, N.; Scalmani, G.; Barone, V. Energies, Structures, and Electronic Properties of Molecules in Solution with the C-PCM Solvation Model. *J. Comput. Chem.* **2003**, *24*, 669–681.

(37) Becke, A. D. Density-Functional Thermochemistry. III. The Role of Exact Exchange. *J. Chem. Phys.* **1993**, *98*, 5648–5652.

(38) Lee, C.; Yang, W.; Parr, R. G. Development of the Colle-Salvetti Correlation-Energy Formula into a Functional of the Electron Density. *Phys. Rev. B: Condens. Matter Mater. Phys.* **1988**, *37*, 785–789.

(39) Bauernschmitt, R.; Ahlrichs, R. Treatment of Electronic Excitations within the Adiabatic Approximation of Time Dependent Density Functional Theory. *Chem. Phys. Lett.* **1996**, *256*, 454–464.

(40) Frisch, M. J.; Trucks, G. W.; Schlegel, H. B.; Scuseria, G. E.; Robb, M. A.; Cheeseman, J. R.; Scalmani, G.; Barone, V.; Mennucci, B.; Petersson, G. A.; Nakatsuji, H.; Caricato, M.; Li, X.; Hratchian, H. P.; Izmaylov, A. F.; Bloino, J.; Zheng, G.; Sonnenberg, J. L.; Hada, M.; Ehara, M.; Toyota, K.; Fukuda, R.; Hasegawa, J.; Ishida, M.; Nakajima, T.; Honda, Y.; Kitao, O.; Nakai, H.; Vreven, T.; Montgomery, J. A., Jr.; Peralta, J. E.; Ogliaro, F.; Bearpark, M.; Heyd, J. J.; Brothers, E.; Kudin, K. N.; Staroverov, V. N.; Kobayashi, R.; Normand, J.; Raghavachari, K.; Rendell, A.; Burant, J. C.; Iyengar, S. S.; Tomasi, J.; Cossi, M.; Rega, N.; Millam, J. M.; Klene, M.; Knox, J. E.; Cross, J. B.; Bakken, V.; Adamo, C.; Jaramillo, J.; Gomperts, R.; Stratmann, R. E.; Yazyev, O.; Austin, A. J.; Cammi, R.; Pomelli, C.; Ochterski, J. W.; Martin, R. L.; Morokuma, K.; Zakrzewski, V. G.; Voth, G. A.; Salvador, P.; Dannenberg, J. J.; Dapprich, S.; Daniels, A. D.; Farkas, Ö.; Foresman, J. B.; Ortiz, J.; Cioslowski, J.; Fox, D. J. *Gaussian 09*; Gaussian Inc.: Wallingford CT, 2009.

(41) O'Boyle, N. M.; Tenderholt, A. L.; Langner, K. M. cclib: A library for package-independent computational chemistry algorithms. *J. Comput. Chem.* **2008**, *29*, 839–845.

(42) Benesi, H. A.; Hildebrand, J. H. A Spectrophotometric Investigation of the Interaction of Iodine with Aromatic Hydrocarbons. *J. Am. Chem. Soc.* **1949**, *71*, 2703–2707.

(43) Saha, U.; Yasmeen Khan, A.; Bhuiya, S.; Das, S.; Fiorillo, G.; Lombardi, P.; Suresh Kumar, G. Targeting Human Telomeric DNA Quadruplex with Novel Berberrubine Derivatives: Insights from Spectroscopic and Docking Studies. *J. Biomol. Struct. Dyn.* **2019**, *37*, 1375–1389.

(44) Saha, U.; Das, B.; Dolai, M.; Butcher, R. J.; Suresh Kumar, G. Adaptable DNA-Interactive Probe Proficient at Selective Turn-On Sensing for Al³⁺: Insight from the Crystal Structure, Photophysical Studies, and Molecular Logic Gate. *ACS Omega* **2020**, *5*, 18411–18423.

(45) Arunagiri, S.; Maiya, B. G. Electro-photo switch” and “Molecular light switch” devices based on Ruthenium(II) complexes of modified dipyrrophenazine ligands: Modulation of the photochemical function through ligand design. *Inorg. Chem.* **1999**, *38*, 842–843.

(46) Abdel-Rahman, L. H.; El-Khatib, R. M.; Nassr, L. A. E.; Abu-Dief, A. M.; Ismael, M.; Seleem, A. A. Metal based pharmacologically active agents: synthesis, structural characterization, molecular modeling, CT-DNA binding studies and in vitro antimicrobial screening of iron(II) bromosalicylidene amino acid chelates. *Spectrochim. Acta, Part A* **2014**, *117*, 366–378.

(47) Abu-Dief, A. M.; Nassr, L. A. E. Tailoring, physicochemical characterization, antibacterial and DNA binding mode studies of Cu(II) Schiff bases amino acid bioactive agents incorporating S-

bromo-2-hydroxybenzaldehyde. *J. Iran. Chem. Soc.* **2015**, *12*, 943–955.

(48) Abu-Dief, A. M.; Abdel-Rahman, L. H.; Shehata, M. R.; Abdel-Mawgoud, A. A. H. Novel azomethine Pd (II)- and VO (II)-based metallo-pharmaceuticals as anticancer, antimicrobial, and antioxidant agents: Design, structural inspection, DFT investigation, and DNA interaction. *J. Phys. Org. Chem.* **2019**, *32*, No. e4009.

(49) Zhou, D.-F.; Chen, Q.-Y.; Qi, Y.; Fu, H.-J.; Li, Z.; Zhao, K.-D.; Gao, J. Anticancer Activity, Attenuation on the Absorption of Calcium in Mitochondria, and Catalase Activity for Manganese Complexes of N-Substituted Di(picolyl)amine. *Inorg. Chem.* **2011**, *50*, 6929–6937.

(50) Pjura, P. E.; Grzeskowiak, K.; Dickerson, R. E. Binding of Hoechst 33258 to the Minor Groove of B-DNA. *J. Mol. Biol.* **1987**, *197*, 257–271.